JPEDAV (2004) 25:497-506
DOI: 10.1361/15477030420962
1547-7037/$19.00 ©ASM International

Review Paper

Crystallography and Phase Equilibria A Review: Part II—Space Groups and Structure

J.F. Smith

(Submitted June 18, 2004)

1. Introduction

This is the second part of a three-part review concerning the relationship between crystal structures and phase equilibria. The first part emphasized that the point group symmetries of the macrosymmetry of a well-developed crystal and of one of its lattice points were identical, with one defining the other. It was noted that the macrosymmetry was a projective symmetry, and, although it was capable of determining the directions and relative magnitudes of the lattice parameters and their angular relationships, it was incapable of defining the numerical magnitudes. Such was the status of crystallographic information as the 19th century rolled toward the 20th. It remained for the 20th century to produce a means of quantitatively defining those parameters and a means for determining the positions of individual atoms within a crystal structure.

The present part of the review speaks to the utilization of diffraction phenomena for establishing the magnitudes and directions of the lattice parameters and to the determination of the atomic loci within crystal structures. In particular, the interest is in the scattering of waves the wavelength of which is near the dimensions of the scattering particles. This type of scattering is known as Thompson scattering, and appropriate wavelengths for scattering by atoms can be found in x-ray, electron, and neutron radiation. In comparison, the scattering by particles that are small with respect to the wavelength of the incident radiation is known as Rayleigh scattering, and the sunbeams produced as visible sunlight passes through a cloud or shines through a window into a room with dust in the air are examples of Rayleigh scattering. The phenomenon is useful for studying colloidal suspensions. It is not the aim of the present review to make expert crystallographers, but rather to make crystallographic information more understandable in terms of its relevance to thermodynamics and phase equilibria. Specific topics that are discussed are as follows:

- Wave motion and its interaction with three-dimensional crystal lattices to produce diffraction patterns in much the same way that sunlight interacts with a ruled grating to produce the colors of the rainbow.
- The positions of diffraction maxima and evaluation of the magnitudes of lattice parameters and inference of space group symmetry.
- Only for very simple structures is it possible to determine atomic positions solely from the positions of diffraction maxima. Furthermore, the inference of a unique space group may not be possible because diffraction is insensitive to the presence or absence of a center of symmetry.
- The intensities of diffraction maxima provide the means of determining the atomic positions within a crystal structure, and symmetry provides limitations upon the number of positional parameters that need to be specified for the atoms.
- Electrons, x-rays, and neutrons are the common radiations that are used in diffraction studies. Electrons and x-rays are diffracted by the electron distributions in materials, so their diffraction data can be used to provide electron density maps where the density maxima imply atomic loci. On the other hand, neutrons are scattered by atomic nuclei and, because the neutron has a magnetic moment, also by magnetic dipoles. Thus, neutron diffraction can yield data that differ from data obtained from x-ray or electron diffraction.

2. Crystal Diffraction

Coherent Thompson scattering is the basis of diffraction. Diffraction effects can be used to distinguish the nature and magnitudes of the translational repetitions in a crystal that projectively cannot be distinguished from simpler inversion, rotational, and mirror symmetries. Various centering conditions of the Bravais lattices provide examples of translations that are readily detectable by diffraction. In addition, there are symmetries that have become known as screw axes and glide planes. These symmetries are a combination of translation and rotation or of mirroring plus translation. The details of these symmetries are subsequently elaborated. Inclusion of these symmetry elements expands the 32 point groups to a total of 230 space group symmetries. The symmetry constraints of a space group make easier the task of defining atomic coordinates and of determining the positional locations of atoms in crystal structures. It should be noted that the space group symmetry of a crystal structure may be inferred from the positions of the diffraction maxima, but that the atomic coordinates are determined from the intensities of the diffraction maxima.

It was the discovery of x-rays by Roentgen in 1895 in combination with the concept of the nuclear atom, derived from the α-particle scattering experiments of Rutherford in the first decade of the 20th century, that stimulated Max von Laue, in early 1912, to irradiate crystals with x-rays. The results confirmed that x-rays, like visible light, were electromagnetic radiation and that the periodic atomic arrays in crystals act as three-dimensional gratings to produce diffraction maxima. W.L. Bragg learned of von Laue's work and performed a series of experiments to produce results

J.F. Smith, J.F. Smith Consulting Services, 2919 S. Riverside Dr., Ames, IA 50010, E-mail: jfsmith@iastate.edu.

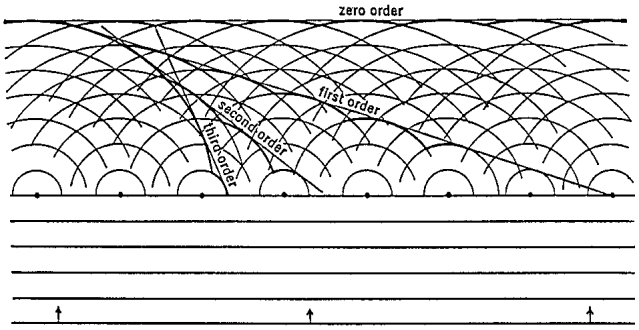

Fig. II-1 Scattering of waves by a periodic array to produce constructive interference in specific directions

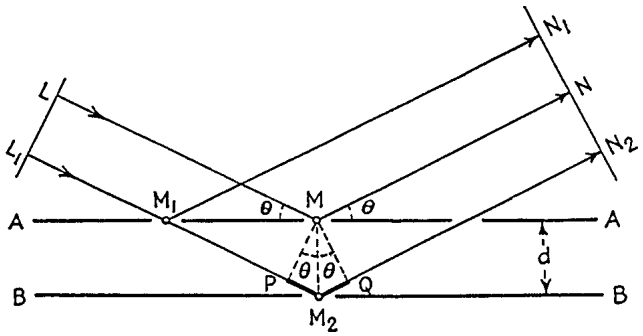

Fig. II-2 Relationship of the interplanar *d*-spacing and the angle θ, which produces a path length difference of $PM_2Q = n\lambda$ between scattering from plane A and plane B

from which were developed a relationship between x-ray wavelength and crystal spacings. These experiments utilized a spectrometer for the determination of x-ray wavelengths that was developed by the father of W.L. Bragg, W.H. Bragg. The resultant relationship is what is now known as Bragg's law, and it defines the conditions that produce diffraction maxima. This law is defined mathematically as

$$\lambda = 2\, d_{hkl} \sin \theta_{hkl}$$

where λ is the x-ray wavelength, θ is the angle between the incident x-ray beam and the scattering lattice planes, and d_{hkl} is the interplanar spacing between the lattice planes. For this discovery, the two Braggs were awarded the Barnard Gold Medal of the U.S. Academy of Sciences in 1914 and the Nobel Prize in Physics in 1915.

In Fig. I-2 from the first part of this review series, it is evident how the lattice points give rise to planar arrays of points that can scatter incident radiation. Figure II-1 in this part of the review illustrates how an advancing wave front, shown by the lower straight lines, is scattered by lattice points. Each point scatters the incident wave over a spherical solid angle. Wave crests pass in succession at intervals of one wavelength, λ. The wave crests that have passed the line of points are shown by the circular arcs whose radii are λ, 2λ, 3λ, to *n*λ. It is evident that, along a general direction, the scattered waves have a random phase relationship, but along the directions indicated by zero order, first order, second order, etc., the scattered waves are in phase, and these are directions of diffraction maxima.

Figure II-2 illustrates how Bragg's law relates to crystal diffraction. In this figure, L-L_1 represents the incident wave front and N_1-N-N_2 represents the scattered wavefront. M_1, M, and M_2 are scattering points along (*hkl*) planes separated by a distance, d_{hkl}. When θ_{hkl} is such that the distance PM_2Q is equal to an integral number of wavelengths, the incident and diffracted waves are in phase and produce a diffraction maximum. In crystallography, it is common to account for higher order diffraction maxima by modifying the *d*-spacing rather than by writing an integer times the wavelength (e.g., for (100) planes the first-order maximum would be for d_{100}, the second-order maximum d_{200}, and the third-order maximum d_{300}).

3. Positions of Diffraction Maxima

The indexing of diffraction maxima in terms of assigning the (*hkl*) planes responsible for the geometric spacings of the diffraction maxima depends upon the experimental apparatus that was used to generate the pattern. Since this review is intended to review crystallographic information with pertinence to alloy phase equilibria, the details of indexing will be left to the crystallographer. Computer programs do exist for indexing powder patterns: A widely used example is the Rietveld program (Ref 1) (powder is herein used to denote fine-grained material with random grain orientation so that all (*hkl*) planes are in a position to contribute to the diffraction pattern). The indexing of a diffraction pattern defines the crystal system of the diffracting material. Then, with the positions of the *hkl* diffraction maxima and the wavelength of the incident radiation both known, Bragg's law may be used to evaluate the magnitudes and angular relationships of the lattice parameters, as shown in Table II-1 for the various crystal systems.

Because volume is relevant to thermodynamic considerations, those interested in phase equilibria may be interested in the volume of a phase under consideration. The volume of a unit cell is the triple scalar product of the lattice parameter vectors. The atomic content of the unit cell in combination with the volume of the unit cell allows the evaluation of the molar volume of a crystalline material. To obtain precise values of the lattice parameters, the Bragg equation may be used to determine the type of measurement to be made. With recognition that the measurement is of θ, the Bragg equation can be rewritten as

$$d \sin \theta = \lambda/2$$

and differentiation leads to

$$d \cos \theta\, \delta\theta + \sin \theta\, \delta d = 0$$

which can be rearranged to

$$\delta d/d = -\cot \theta\, \delta\theta$$

Table II-1 Relationships between *d* spacings for *hkl* reflections and lattice parameters for the seven crystal systems

Cubic system:

$$d = \frac{a}{\sqrt{h^2 + k^2 + l^2}}$$

Tetragonal system:

$$d = \frac{1}{\sqrt{\frac{h^2}{a^2} + \frac{k^2}{a^2} + \frac{l^2}{c^2}}}$$

Orthorhombic system:

$$d = \frac{1}{\sqrt{\frac{h^2}{a^2} + \frac{k^2}{b^2} + \frac{l^2}{c^2}}}$$

Hexagonal system, hexagonal indexing:

$$d = \frac{1}{\sqrt{\frac{4}{3a^2}(h^2 + k^2 + hk) + \frac{l^2}{c^2}}}$$

Hexagonal system, rhombohedral indexing:

$$d = \frac{1}{\frac{1}{a}\sqrt{\frac{(h^2 + k^2 + l^2)\sin^2\alpha + 2(hk + hl + kl)(\cos^2\alpha - \cos\alpha)}{1 + 2\cos^3\alpha + 3\cos^2\alpha}}}$$

Monoclinic system:

$$d = \frac{1}{\sqrt{\frac{\frac{h^2}{a^2} + \frac{l^2}{c^2} - \frac{2hl}{ac}\cos\beta}{\sin^2\beta} + \frac{k^2}{b^2}}}$$

Triclinic system:

$$d = \sqrt{\frac{\begin{vmatrix} \frac{h}{a} & \cos\gamma & \cos\beta \\ \frac{k}{b} & 1 & \cos\alpha \\ \frac{l}{c} & \cos\alpha & 1 \end{vmatrix} + \frac{k}{b}\begin{vmatrix} 1 & \frac{h}{a} & \cos\beta \\ \cos\gamma & \frac{k}{b} & \cos\alpha \\ \cos\beta & \frac{l}{c} & 1 \end{vmatrix} + \frac{l}{c}\begin{vmatrix} 1 & \cos\gamma & \frac{h}{a} \\ \cos\gamma & 1 & \frac{k}{b} \\ \cos\beta & \cos\alpha & \frac{l}{c} \end{vmatrix}}{\begin{vmatrix} 1 & \cos\gamma & \cos\beta \\ \cos\gamma & 1 & \cos\alpha \\ \cos\beta & \cos\alpha & 1 \end{vmatrix}}}$$

Since cot θ varies from infinity at θ = 0 to become asymptotically zero at θ = 90°, the import of this equation is that it indicates that errors in the measurement of θ become less and less important in the evaluation of *d* as θ increases toward 90°. Unfortunately, the physical limitations of construction prevent building an apparatus to accumulate diffraction data at angles much greater than θ = 75° to 80°. Even so, precisions of 0.1 to 0.2% (four significant figures) are readily obtained from back reflection data, and with great care a fifth significant figure is attainable.

4. Atomic Arrays and Diffracted Waves

There are many factors that affect the intensity of diffracted waves (e.g., temperature, absorption, etc.). However, the factor of most interest to the crystallographer is the geometry of the atomic array within a crystal. This relates to the bonding interactions and thence to the energetics that stabilize the crystal. For purposes of unraveling the nature of this geometry, relative intensities of the diffracted maxima are sufficient. For an "ideally imperfect" solid, the diffracted intensites, I_{hkl}, are proportional to the square of the absolute magnitude of a quantity that is called the structure factor, F_{hkl}. For a truly perfect solid, the Bragg conditions would be satisfied both in the incident and diffracted directions leading to attenuation arising from internal diffraction back and forth between the incident and diffracted directions. The ultrastrong "whiskers" that received so much study a few decades ago probably approach this level of perfection.

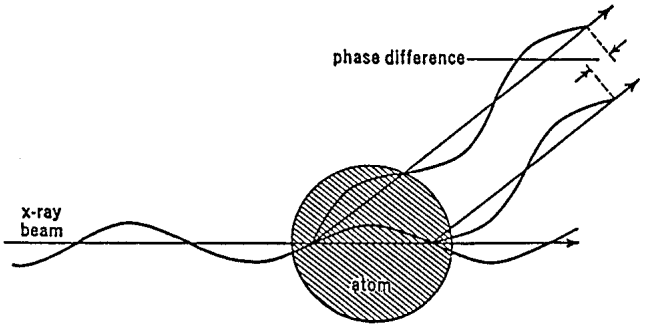

Fig. II-3 The atom factor arises from the phase shift induced by the fact that the incident wave maximum passes a point in front of an atom at a different time than it passes a point on the far side of the atom.

Though the intensity from a truly perfect crystal should be directly proportional to $|F_{hkl}|$ rather than $|F_{hkl}|^2$, ordinary crystals contain enough imperfections in the form of dislocations, vacancies, foreign atoms, and misplaced atoms, etc., to cause warpage of the atomic planes to reduce multiple diffraction back and forth between planes, so ordinary crystals can be classified as ideally imperfect with I_{hkl} being proportional to $|F_{hkl}|^2$. It may be noted at this point that, if conditions for diffraction are met in a given direction, they are also met at 180° from that direction. Thus, a diffraction pattern does not distinguish between top and bottom, front and back, or left and right sides, and is therefore incapable of detecting the presence or absence of a center of symmetry. However, a statistical analysis of the intensity distributions can show whether or not a center of symmetry is present (Ref 2).

The structure factor involves two terms; one of these is the atom factor, and the other depends upon the geometric distances and directions of the atomic separations within the lattice point. The scattering of x-rays and electrons is dependent upon the electronic distribution around an atom, and for those two radiations the atom factors are the same. However, neutrons are scattered by the nuclei and by magnetic moments, so the atom factors for neutrons are different and for present purposes are discussed in detail. That part of the incident wave that continues in the same direction as the incoming wave (zero-order wave front in Fig. II-1) has no phase shifting, so the atom factor is simply the number of electrons around an atom (i.e., the atomic number). For all other directions of scattering, there is a phase shift between scattering from an electron in one position compared with an electron at a different position. This is illustrated in Fig. II-3. The attenuation due to the phase shifting of all electrons in the atom is the atom factor, *f*.

For x-rays and electrons, a plot of atom factors for hydrogen through uranium are plotted as functions of $(\sin \Theta)/\lambda$ in Fig. II-4. This plot illustrates that the determination of the positions of light atoms in the crystal structures of phases with light atoms combined with heavy atoms is difficult because the intensities in such a diffraction pattern are dominated by the heavy atoms, with only minor contribution from the light atoms. It may also be noted that if there is a level of ionization of an atom, the zero intercept of the atom factor should rise or fall by the level of ionization. However, any level of ionization involves the outermost electrons, but Bragg's law shows that diffraction data invert space, in the sense that d_{hkl} and θ_{hkl} are inversely related. Thus, as $(\sin \theta_{hkl})/\lambda$ increases, the importance of the valence electrons rapidly decreases and the core electrons dominate to make the atom factor insensitive to any level of ionization except in the very far front reflection region. Indeed, it requires a great deal of work to get any information on the bonding electron configuration from diffraction studies (Ref 3).

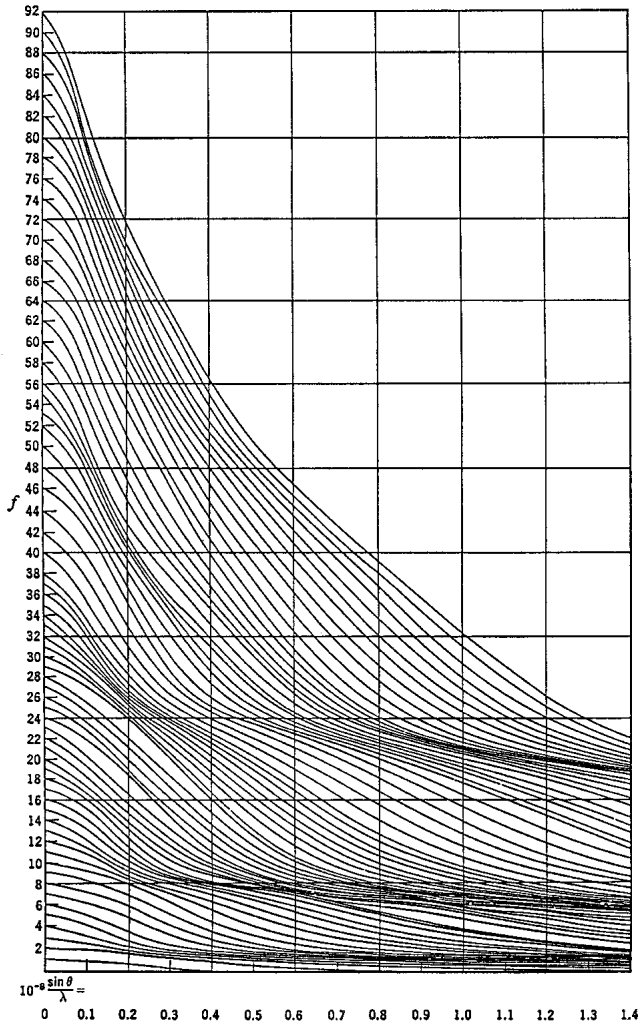

Fig. II-4 A plot of the atom factors for the 92 naturally occurring atoms

The other term in the structure factor has to do with the vectorial relationships among all of the atoms in the crystal structure and results from the fact that an atom at one position in a unit cell will see the incident wave at a different phase angle than an atom at another position. Thus, the composite of the phase relationships of all atoms in a crystal structure must be considered for each reflection. The structure factor may be written as

$$F_{hkl} = \Sigma_i f_i \exp 2\pi j(hx_i + ky_i + lz_i)$$

where the summation is over all of the atoms in the unit cell, f_i is the atom factor for the ith atom, hkl are the Miller indices of the reflection, $j = \sqrt{-1}$, and x_i, y_i, and z_i are atomic coordinates in terms of the fractional translations of the lattice parameters to define the locus of the ith atom with respect to the origin of the unit cell.

The availability of a quantitative expression related to the intensity of hkl reflections allows the crystallographer to search diffraction data for characteristic extinctions. Such characteristic extinctions carry information concerning the translational relationships within a crystal. How and why this works can be illustrated by examining centering constraints upon diffraction intensities. A very simple case is a body-centered Bravais lattice. With recognition that a body-centered lattice, **I**, repeats everything in the array of one lattice point at a translation of (**a** + **b** + **c**)/2, the structure factor may be rewritten as

$$F_{hkl} = \Sigma_i f_i \exp 2\pi j \{(hx_i + ky_i + lz_i) + (h[x_i + ½] + k[y_i + ½] + l[z_i + ½])\}$$

where the summation is now over the atoms in one-point array rather than over every atom in the unit cell. Since $\exp(a + b) = (\exp a)(\exp b)$, a common factor in the two terms is $\Sigma_i f_i \exp 2\pi j \{(hx_i + ky_i + lz_i)\}$, so the structure factor can be rewritten as

$$F_{hkl} = \{1 + \exp \pi j (h + k + l)\} \Sigma_i f_i \exp 2\pi j (hx_i + ky_i + lz_i)$$

Series expansion shows that $\exp \pm j\phi = \cos \phi \pm j \sin \phi$. Since h, k, and l are integers, the conversion of $\exp \pi j (h + k + l)$ to a cos and sin representation results in the $\sin (h + k + l)\, \pi = 0$. Because h, k, and l are integers, the cos term will be 1 if $(h + k + l)$ is even or -1 if $(h + k + l)$ is odd. If odd, $\{1 + \exp \pi j (h + k + l)\}$ will be zero, and the diffraction pattern of a body-centered lattice will show no diffraction maxima for which the sum of the Miller indices are odd. Analogous procedures can be used to derive conditions for non-extinctions of hkl reflections for non-primitive lattices, i.e., face-centered (F), end-centered (A, B, or C), hexagonal indexing of a rhombohedral lattice (R), and rhombohedral indexing of a hexagonal lattice (H). Table II-2 summarizes the conditions for non-extinction.

To understand all of the listings in Table II-2, a discussion of glide planes and screw axes is necessary. A glide plane is a mirror plane with the reflected plane being translated with respect to its mirror image. In other words, a mirrored plane has exactly the same atomic content and geometry as the plane from which it reflects, but there is a displacement of one plane with respect to another. The external form of a crystal containing glide planes is unaffected by such displacement, but x-ray reflections can detect their presence. As an example, if the glide plane is normal to the **a** direction, a general point at xyz will involve a reflection that changes x to $\bar{x}$, and y and/or z is translated. If y is translated, the new point occurs at $\bar{x}, y + ½, z$ and this is known as a **b** glide. The detection of this glide plane is in the $0kl$ reflections, a subset of the general hkl reflections. The structure factor for $0kl$ reflections with a **b** glide can be written as

$$F_{0kl} = \Sigma_i f_i \exp 2\pi j \{ky_i + lz_i + k(y_i + ½) + lz_i\}$$

which with rearrangement is

$$F_{0kl} = \{1 + \exp \pi jk\} \Sigma_i f_i \exp 2\pi j (ky_i + lz_i)$$

so $F_{0kl} = 0$ if k is odd. A **b** glide can occur in a P, B, or C bravais lattice.

Other extinctions in $0kl$ reflections are indicative of other types of glides e.g., k mixed, $l = 2n$ indicates a **c** glide with translation $z_i + ½$; $k + l = 2n$ indicates an **n** glide with translations $y_i + ½$ and $z_i + ½$; and $k + l = 4n$ indicates a **d** glide with ¼ translations and with x reversing signs at each ¼ translation. Figure II-5a illustrates an **n** glide normal to the **a** direction, and Fig. II-5b illustrates a **d** glide normal to the **b** direction.

Combinations of rotations and translations lead to screw axes. When viewed down the axis, a screw axis projects as simple rotation. A twofold screw axis parallel to the c axis takes a general point at xyz to $\bar{x},\bar{y},z + ½$. Repetition of this operation produces a second point at one lattice translation from the original point. Note that there is no right- or left-handed sense to this axis because a 180° turn in either sense is the same, and such a twofold screw axis is designated as 2_1. However, threefold, fourfold, and sixfold screw axes may be left-handed or right-handed. A threefold screw axis that is left-handed, 3_1, takes a general point xyz first to $\bar{y},x - y,z + ⅓$, then to $y - x,\bar{x},z + ⅔$, while a right-handed rotation reverses the sequence with xyz going first to $y - x,\bar{x},z + ⅓$ and then to $\bar{y},x - y,z + ⅔$, and is designated as a 3_2 screw axis. Threefold, fourfold, and sixfold screw axes are compared with simple rotors and rotation inversion rotors in Fig. II-6. Note that 4_2 and 6_3, like 2_1, are neither right- nor left-handed. Note also that all screw axes project onto a plane normal to the rotation axis as simple rotors of the same rotation number and are therefore not detectable in macrosymmetry. The presence or absence of screw axes may be inferred from the extinctions in the subsets of the $h00$, $0k0$, $00l$, or $hh0$ reflections (Table II-2). In the case of left-handed and right-handed screw axes, they may also be detected by the measurement of physical properties such as the rotation of polarized light. In some instances, left-handed and right-handed screw axes may also explain some enantiomorphic twinning.

5. Determining Space Group and Crystal Structure

To illustrate the utility of symmetry, the crystal structure determination (Ref 4) of the phase $Ni_{10}Zr_7$ is reviewed. A study of the phase diagram (Ref 5) of the Ni-Zr system has reported a range of homogeneity for this phase extending

Table II-2 Characteristic extinction and non-extinction conditions for the various symmetry elements that involve translational components

Class of reflection	Condition for non-extinction (n = an integer)	Interpretation of extinction	Symbol of symmetry element
hkl	$h + k + l = 2n$	Body-centered lattice	I
	$h + k = 2n$	C-centered lattice	C
	$h + l = 2n$	B-centered lattice	B
	$k + l = 2n$	A-centered lattice	A
	$\circlearrowleft$ $h, k, l,$ all even or all odd	Face-centered lattice	F
	$-h + k + l = 3n$	Rhombohedral lattice indexed on hexagonal reference system	R
	$h + k + l = 3n$	Hexagonal lattice indexed on rhombohedral reference system	H
$0kl$	$k = 2n$	(100) glide plane, component $\frac{b}{2}$	b (P, B, C)
	$l = 2n$	(100) glide plane, component $\frac{c}{2}$	c (P, C, I)
	$k + l = 2n$	(100) glide plane, component $\frac{b}{2} + \frac{c}{2}$	n (P)
	$k + l = 4n$	(100) glide plane, component $\frac{b}{4} + \frac{c}{4}$	d (F)
$h0l$	$h = 2n$	(010) glide plane, component $\frac{a}{2}$	a (P, A, I)
	$l = 2n$	(010) glide plane, component $\frac{c}{2}$	c (P, A, C)
	$h + l = 2n$	(010) glide plane, component $\frac{a}{2} + \frac{c}{2}$	n (P)
	$h + l = 4n$	(010) glide plane, component $\frac{a}{4} + \frac{c}{4}$	d (F), (B)
$hk0$	$h = 2n$	(001) glide plane, component $\frac{a}{2}$	a (P, B, I)
	$k = 2n$	(001) glide plane, component $\frac{b}{2}$	b (P, A, B)
	$h + k = 2n$	(001) glide plane, component $\frac{a}{2} + \frac{b}{2}$	n (P)
	$h + k = 4n$	(001) glide plane, component $\frac{a}{4} + \frac{b}{4}$	d (F)
hhl	$l = 2n$	$(1\bar{1}0)$ glide plane, component $\frac{c}{2}$	c (P, C, F)
	$h = 2n$	$(1\bar{1}0)$ glide plane, component $\frac{a}{2} + \frac{b}{2}$	b (C)
	$h + l = 2n$	$(1\bar{1}0)$ glide plane, component $\frac{a}{4} + \frac{b}{4} + \frac{c}{4}$	n (C)
	$2h + l = 4n$	$(1\bar{1}0)$ glide plane, component $\frac{a}{2} + \frac{b}{4} + \frac{c}{4}$	d (I)
$h00$	$h = 2n$	[100] screw axis, component $\frac{a}{2}$	2_1, 4_1
	$h = 4n$	[100] screw axis, component $\frac{a}{4}$	4_1, 4_3
$0k0$	$k = 2n$	[010] screw axis, component $\frac{b}{2}$	2_1, 4_3
	$k = 4n$	[010] screw axis, component $\frac{b}{4}$	4_1, 4_3
$00l$	$l = 2n$	[001] screw axis, component $\frac{c}{2}$	2_1, 4_2, 6_3
	$l = 3n$	[001] screw axis, component $\frac{c}{3}$	3_1, 3_2, 6_2, 6_4
	$l = 4n$	[001] screw axis, component $\frac{c}{4}$	4_1, 4_3
	$l = 6n$	[001] screw axis, component $\frac{c}{6}$	6_1, 6_2
$hh0$	$h = 2n$	[110] screw axis, component $\frac{a}{2} + \frac{b}{2}$	2_1

from near 56.5 to 58.9 at.% Ni. The latter corresponds within experimental uncertainty with the stoichiometric composition. Two small crystals were grown in this phase, one at the Ni-rich (stoichiometric) boundary and one at the Zr-rich boundary. Diffraction symmetries were compatible with orthorhombic symmetries for both crystals, and precision lattice parameter determinations are shown in Table II-3. The densities of massive samples were found to be 7.78 g/cm^3 for a 48 wt.% Ni alloy and 7.67 g/cm^3 for a 45.3 wt.% Ni alloy. These compositions are very near the phase boundaries.

With the formula $Ni_{10}Zr_7$ and the volume of the unit cell from the lattice parameters, a theoretical density of 7.79 g/cm^3 is obtained with four formula masses per unit cell for the stoichiometric phase. The phase diagram shows the Zr-rich phase boundary to be 45.5 wt.% Ni, which, with substitutional replacement of two smaller Ni atoms by two larger Zr atoms, generates a unit cell with composition $Ni_{38}Zr_{30}$ with a theoretical density of 7.68 g/cm^3. Both theoretical densities are slightly larger than the experimental densities, which is the norm because massive samples contain grain boundaries and other imperfections that tend to reduce the density. The lattice parameters for the Zr-rich phase are larger than those of the stoichiometric phase, which is compatible with the substitutional replacement of smaller Ni atoms by larger Zr atoms.

The positions and intensities of 289 independent reflections were measured for the Zr-rich crystal and of 172

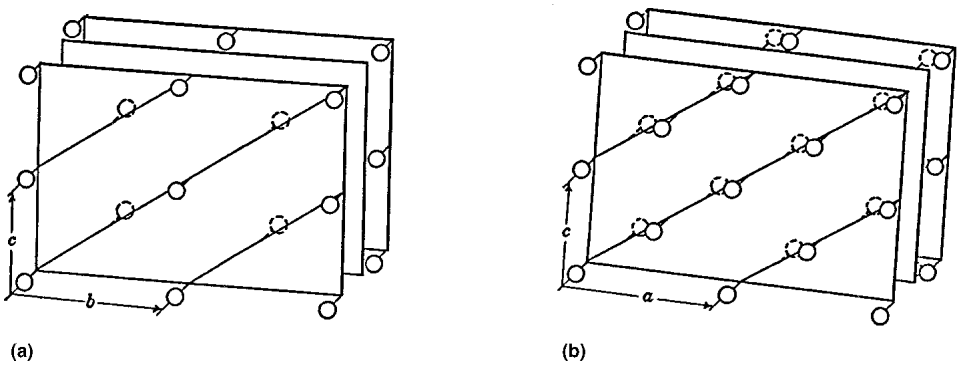

Fig. II-5 In both cases, a glide plane is shown with replications by unit translations in all three directions. **(a)** An illustration of an **n** glide normal to the **a** direction. In this case, 0*kl* reflections would occur only with $k + l = 2n$, and each point would be duplicated by changing the sign of x and translation both y and z by ½. **(b)** An illustration of a **d** glide normal to the **b** direction. In this case, *h*0*l* reflections only with $h + 1 = 4n$, and each point would be duplicated by changing the sign of y and translating x and z by ¼.

independent reflections for the stoichiometric phase. For the Zr-rich crystal, no characteristic extinctions were observed in the general set of (*hkl*) reflections. Thus, the lattice was taken to be primitive **P**. However, (0*kl*) reflections occurred only with $k = 2n$, (*h*0*l*) reflections occurred only with $l = 2n$, and (*hk*0) reflections occurred only with $h = 2n$. From Table II-2, it can be seen that these represent, respectively, a **b** glide normal to the **a** direction, a **c** glide normal to the **b** direction, and an **a** glide normal to the **c** direction. Thus, the space group at the Zr-rich boundary is indicated to be *Pbca*.

For the stoichiometric crystal (*hkl*), reflections were observed only when $h + k = 2n$, which is indicative of a **C**-centered lattice. For (0*kl*) reflections, no characteristic extinctions were observed. However, (*h*0*l*) reflections occurred only with $h + l = 2n$. C centering requires $h + k = 2n$, so h must equal $2n$ when $k = 0$, then so also must $1 = 2n$. The latter was taken as indicating a **c** glide normal to the **b** direction. The (*hk*0) reflections appeared only with both $h = 2n$ and $k = 2n$, but not with two odd values. This might be indicative of either an **a** or **b** glide normal to the **c** direction. By analogy with the Zr-rich crystal, an **a** glide seems more likely, so the probable space group was taken to be *C*2*ca* or *Cmca*. The former lacks a center of symmetry, but the latter has one.

The determination of the crystal structure of the Zr-rich crystal was done first. After making standard corrections to the intensity data so that I_{hkl} is proportional to $|F_{hkl}|^2$, Patterson projections were made for the (x,y), (x,z), and (y,z) planes. These projections are simply plots of the function $P(x,y) = \Sigma\ |F_{hkl}|^2 \cos 2\pi(hx + ky)$ evaluated at incremental values of x and y across a unit cell. $P(x,z)$ and $P(y,z)$ are analogous. With modern computing capability, this would have been done today with a three-dimensional Patterson projection. These plots provide information with regard to the interatomic vectors, which are inferred from the distances and directions from the origin to the various maxima that appear in the summations. Reference to the *International Tables for X-ray Crystallography* shows that space group *Pbca* has its symmetry satisfied by the occupancy of either of two fourfold special sets or eightfold general sets as follows:

4(a) 000; ½,½,0; 0,½,½; ½,0,½

4(b) 0,0,½; ½,½,½; 0,½,0; ½,0,0

8(c) xyz; $\frac{1}{2}+x,\frac{1}{2}-y,\bar{z}$; $\bar{x},\frac{1}{2}+y,\frac{1}{2}-z$; $\frac{1}{2}-x,\bar{y},\frac{1}{2}+z$;
$\bar{x}\bar{y}\bar{z}$; $\frac{1}{2}-x,\frac{1}{2}+y,z$; $x,\frac{1}{2}-y,\frac{1}{2}+z$; $\frac{1}{2}+x,y,\frac{1}{2}-z$

Such sets are normally termed Wykoff sets.

With the four formula weights per unit cell indicated by density considerations, these sets were utilized to find locations of 40 Ni sites and 28 Zr sites. Note that once either fourfold set is occupied there is no possibility of using it again, but by choosing different xyz coordinates the eightfold sets can be used many times. The stoichiometry requires that one fourfold set must be occupied by Zr and limits the choice for the remaining Zr atoms to 8(c) sets. After several unsuccessful attempts, a suitable trial structure was derived that satisfactorily matched the Patterson projections, had reasonable interatomic spacings, and gave reasonable agreement between the calculated and observed structures. This structure was refined by the method of least squares to yield the following reliability indices with subscript o being based on observed intensity data and c being calculated with the refined positional parameters

$$R_1 = \Sigma\big||F_o| - |F_c|\big|/\Sigma|F_o| = 0.163 \text{ and}$$
$$R_2 = \Sigma(|F_o| - |F_c|)^2/\Sigma F_0^2 = 0.0330$$

The refined structure utilized the 4(a) set and three eightfold sets for Zr and five eightfold sets for Ni and required the adjustment of 24 positional parameters.

Once the structure of the Zr-rich phase had been refined, it was relatively easy to postulate trial structures for the stoichiometric phase in both space groups *Cmca* and *C*2*ca*. However, the trial structure in the centrosymmetric space group *Cmca* did not refine below a reliability factor of $R_1 = 0.399$, whereas the trial structure in space group C2*ca* readily refined to $R_1 = 0.166$ and $R_2 = 0.023$. For space group *C*2*ca*, there are again only fourfold and eightfold sets, in this case one of each:

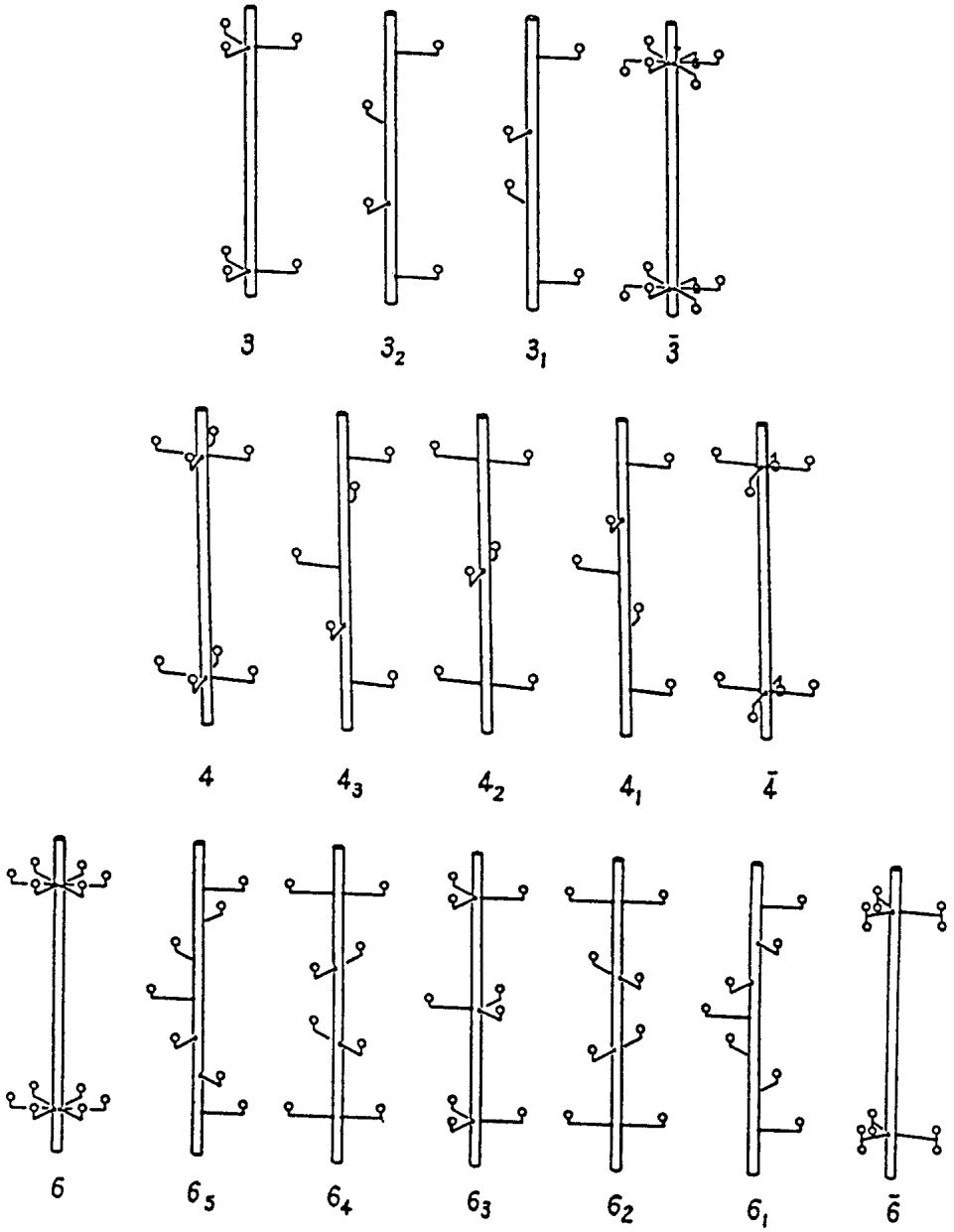

Fig. II-6 Comparison of the various kinds of threefold, fourfold, and sixfold rotational symmetry. For each set, it is evident that all threefold, fourfold, or sixfold rotors project as simple rotors.

4(a) $x,0,0;\ ½ + x,½,0;\ ½ + x,0,½;\ x,½,½$

8(b) $xyz;\ ½ + x,½ + y,z;\ ½ + x,y,½ - z;\ x,½ - y,½ + z;$
$\bar{x}\bar{y}\bar{z};\ ½ + x,\ ½ - y,\bar{z};\ x,½ + y,½ - z,\ ½ + x,\bar{y},½ + z$

In *C*2*ca*, there is one adjustable parameter in the fourfold set, so that more than one fourfold set may be utilized. The refined structure showed 12 Zr atoms in three fourfold sets (indicated in Fig. II-7 by subscripts 0, 1a, and 1b), each with a different x positional parameter. The remaining 16 Zr atoms were in two different eightfold sets (subscripted as 2 and 3), while the 40 Ni atoms were in five eightfold sets (subscripted as 4, 5, 6, 7, and 8 in Fig. II-7 and 8). The total number of positional parameters in the refinement was again 24.

Table II-3 Precision lattice parameters for crystals of the stoichiometric and Zr-rich phase boundaries of the $Ni_{10}Zr_7$ phase

Stoichiometric	Zirconium-rich
$a_0 = 1.2386 \pm 0.006$ nm	$a_0 = 1.2497 \pm 0.004$ nm
$b_0 = 0.9156 \pm 0.008$ nm	$b_0 = 0.9210 \pm 0.008$ nm
$c_0 = 0.9211 \pm 0.005$ nm	$c_0 = 0.9325 \pm 0.002$ nm

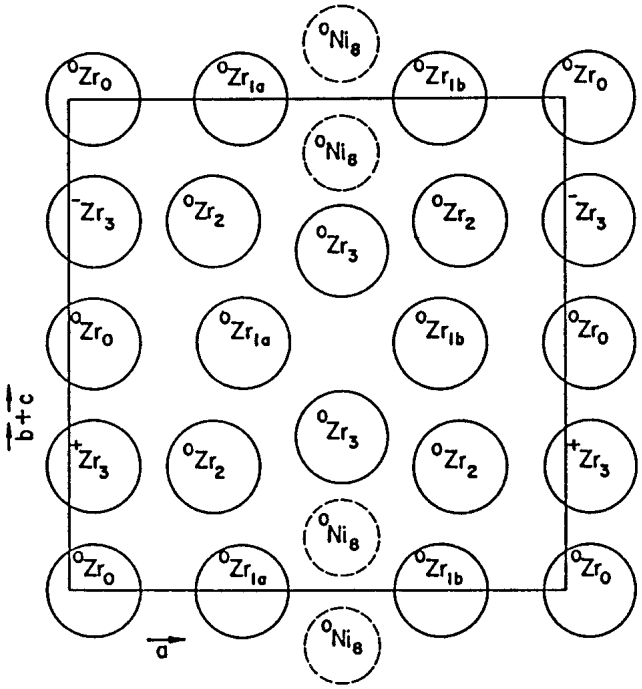

Fig. II-7 The atomic arrangement within the Zr layers is illustrated. The prefixed superscript zero indicates atoms that are coplanar, while the prefixed + and – indicate atoms that are, respectively, above and below the plane. The subscripted numbers represented atoms within related Wykoff sets. If the solid lines represent the lattice parameter translations with the origin at the lower left, the figure represents the geometry of a (011) plane passing through the center of the unit cell. Successive equivalent layers can be generated by the C-centering operation.

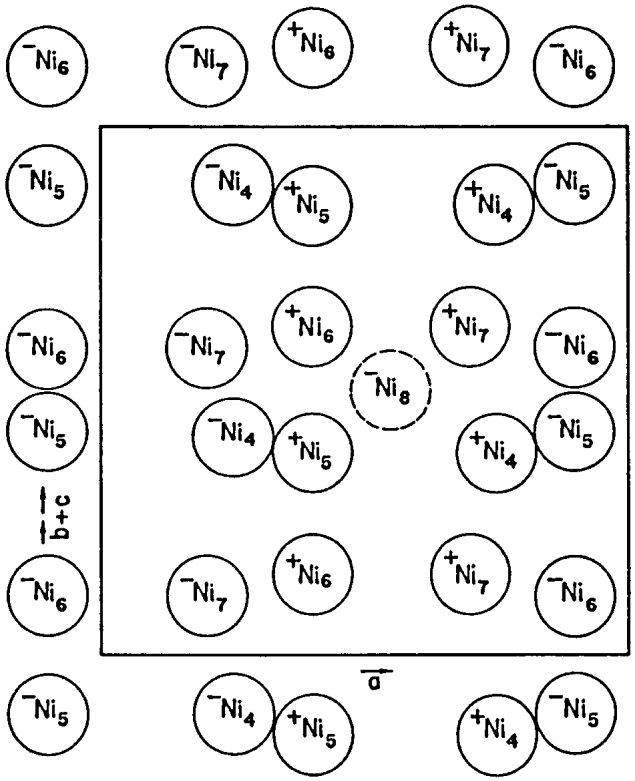

Fig. II-8 The atomic arrangement within the Ni layers that interlay between the successive Zr layers. Again, the prefixed superscripts + and – indicate atoms that are slightly above and below the plane, and the subscript numbers represent atoms within a Wykoff set. If the rectangle in this figure is superimposed over the rectangle in Fig. II-7, the positioning of the Ni atoms will be that of the first Ni layer interposed between the Zr layer of Fig. II-7 and the next Zr layer generated by C-centering.

A comparison of the structures of the stoichiometric phase and the Zr-rich phase showed them to be closely comparable. The basic structure of the stoichiometric phase is shown in Fig. II-7 and II-8 to be an interlayered array with alternate layers of primarily Zr atoms and wrinkled layers solely of Ni atoms. Figure II-7 shows that the Zr in the three fourfold sets all lie at the same level along lines paralleling the **a** lattice parameter at $\mathbf{b} + \mathbf{c} = 0$ and $\mathbf{b} + \mathbf{c} = ½$. The eightfold sets Zr-3 and Ni-8 are also coplanar, but the eightfold set Zr-2 is slightly displaced up and down. The wrinkled Ni layer shown in Fig. II-8 can be superimposed above the layer in Fig. II-7 to develop the three-dimensional structure. Then the structure is completed if the pairs of layers are reproduced by the C-centering operation.

The structure of the Zr-rich crystal differs in that there are significant distortions of the stoichiometric structure. For instance, the fourfold Zr sets no longer lie on a straight line parallel to the **a** axis. Rather with one atom on the **a** axis, the next two are displaced alternately in one direction or the other from the axis so that the 1a and 1b fourfold sets coalesce into an eightfold set. Similar distortional shifts are seen in the coordinates of other sets, so that the C centering is lost to revert to the lower symmetry *Pbca* space group. Thus, this is a case in which there is a continuous phase that changes space groups as composition changes. There is a transition, but it is not first order so it will not appear on an equilibrium diagram. The rules that govern the legitimacy of second-order transitions are discussed in more detail in part III of this review.

6. Summary

- The lengthy discussion of the structure determination of the $Ni_{10}Zr_7$ phase illustrates the utility of symmetry in reducing work. Had there been no use of symmetry, the determination of the structures would have required the determination of the positional coordinates of 68 atoms, or a total of 204 positional parameters. The inclusion of the symmetry constraints reduced this number to 24. This is a reduction in number in excess of eightfold.
- The structure change in $Ni_{10}Zr_7$ shows that a single phase can undergo a shift in space groups for reasons other than order-disorder.
- Once a structure has been refined, it is relatively straightforward to calculate interatomic distances and coordination numbers. This is relevant to the choice of models for computing the variation in phase composition, i.e., substitution, interstitial, or vacancy model. In

the present case, the evidence supports substitution. The question then is which sets are most likely to accept atomic replacement, and the interatomic distances indicate that substitution of Zr for Ni in the Ni-8 set is least likely, but there is little to differentiate the Ni-4 through Ni-7 sets, so a random substitution of Zr for Ni at those 32 loci would seem reasonable.

- Also the atomic coordination in combination with the relative positions of the components in the periodic chart offers clues as to the nature of the bonding in the structure and thence to the expected magnitudes of the enthalpies of formation. In the case of $Ni_{10}Zr_7$, the structure determination indicates that the compound is primarily a packing compound with only secondary directionality considerations. The enthalpy of formation should therefore be normally metallic for the number of valence electrons involved. Again this is discussed in more detail in part III of this review.

References

1. H.M. Rietveld, *Aust. J. Phys.,* Vol 41 (No. 2), 1988, p 113
2. E.R. Howells, D.C. Phillips, and D. Rogers, *Acta Crystallogr.,* Vol 3, 1950, p 310
3. A.E. Ray and J.F. Smith, *Acta Crystallogr.,* Vol 13, 1960, p 645
4. M.E. Kirkpatrick, J.F. Smith, and W.L. Larsen, *Acta Crystallogr.,* Vol 15, 1962, p 894
5. M.E. Kirkpatrick and W.L. Larsen, *Trans. Am. Soc. Met.,* Vol 54, 1964, p 580

Selected Reference

- Dame Kathleen Lonsdale, International Tables for X-ray Crystallography, Kynoch Press, Birmingham, U.K., p 1952-1974